Article

Effect of Transition Metal Elements on High-Temperature Properties of Al–Si–Cu–Mg Alloys

Chao Gao, Lingkun Zhang and Bingrong Zhang *

School of Mechanical & Automotive Engineering, Qilu University of Technology (Shandong Academy of Sciences), Jinan 250353, China; 1043119015@stu.qlu.edu.cn (C.G.); 1043117038@stu.qlu.edu.cn (L.Z.)
* Correspondence: brzit@aliyun.com; Tel.: +86-186-0634-7079

Abstract: In the present work, we studied the effects of transition metal elements on microstructure evolution and high-temperature mechanical properties via the preparation of new modified alloys with micro-additions of Cr, Ti, V, Zr, Mo, and Mn to address the poor high-temperature performance of Al–Si–Cu–Mg alloys for automotive engines. The results show that the addition of transition metal elements formed a variety of new intermetallic phases that were stable at high temperatures, such as $(AlSi)_3(TiVZr)$, $(AlSi)_3Ti$, $(AlSi)_3(CrVTi)$, $Al_{74}Si_6Mn_4Cr_2Fe$, $Al_{85}Si_5Mn_2Mo_2CrFe$, $Al_{0.78}Fe_{4.8}Mn_{0.27}Mo_4.15Si_2$, $(AlSi)_2(CrVTi)Mo$, and $Al_{13}(MoCrVTi)_4Si_4$, and these phases evidently improved the ultimate high-temperature tensile strength and yield strength. The ultimate tensile strength and yield strength of the modified alloy increased by 17.49% and 31.65% when the test temperature increased to 240 °C, respectively, and by 71.28% and 74.73% when the test temperature increased to 300 °C, respectively. The fundamental reason for this change is that the intermetallic phase hinders the expansion of cracks, which can exist stably at high temperatures. When a crack extends to the intermetallic phases, it will break along with the intermetallic phases or propagate along the morphological edge of the intermetallic phases.

Keywords: Al–Si–Cu–Mg alloys; transition metal elements; ultimate tensile strength; yield strength; high-temperature properties

1. Introduction

Al–Si casting alloys are widely used in manufacturing automotive engine cylinder heads due to their advantages of being lightweight, good casting performance, and excellent comprehensive mechanical properties [1]; however, with the contradictory development of high load stress and thin-walled structure of the high-performance engine, the requirements for the balance of strength and toughness at room temperature as well as the high-temperature performance of aluminum alloy cylinder heads and engine blocks are becoming stricter. To meet this market demand, researchers began to study how to achieve better values of both strength and ductility at room temperature and improve the high-temperature performance of Al–Si casting alloys. Li Runxia et al. [2] found that Al–Si alloy's strength and toughness can be improved by adjusting the content of Cu and Mg. According to the literature [3–5], adjusting the Cu/Mg ratio changed the formation process of strengthening phases in Mg_2Si, Q-$Al_5Mg_8Si_4Cu_2$, and θ-Al_2Cu, and thus changed the strength and toughness of the alloy; however, the traditional intermetallic phase such as Mg_2Si, Q-$Al_5Mg_8Si_4Cu_2$, and θ-Al_2Cu phase will coarsen rapidly above 200 °C [6]; therefore, the strengthening effect by these intermetallic phases can remain only at room temperature. To keep the microstructure of the aluminum alloy cylinder head stable and strong at temperatures higher than 200 °C, it is necessary to find micro-alloy elements that can form a thermally stable strengthening phase with the main alloy elements (Al–Si–Cu–Mg) and make the alloy stronger and tougher simultaneously. In recent years, the elements that meet the above conditions are Cr, Ti, V, Zr, Mo, Mn, and other transition metal elements.

Shaha et al. [7] studied the influence of transition metal elements on the high-temperature properties of Al–Si alloys, and pointed out that the micro-alloy elements added to improve the high-temperature properties of Al–Si alloys should meet the following conditions: (1) be capable of forming a thermally stable strengthening phase, (2) have low solid solubility in the Al matrix, (3) have low diffusivity in the Al matrix, and (4) retain the original cooling solidification ability of aluminum alloy. On this basis, Shaha [8] chose to add transition metals Cr, Ti, V, and Zr to the Al–Si–Cu–Mg alloy. It was found that the yield strength (YS) and ultimate tensile strength (UTS) of the modified alloy increased by 30% and 5%, respectively, under the same treatment and test conditions. Then, throughout the addition of Mo and Mn in Al-7Si-1Cu-0.5Mg (wt%) base alloy, it is found that some Mo-rich and Mn-rich intermetallic phases are formed in the alloy, some of them can remain stable after heat treatment, which shows that they can obviously improve the high-temperature properties of the alloy [9]. After T6 heat treatment, the mechanical properties of the alloy with Mo and Mn are better than that of the base alloy at any test temperature (25–300 °C). Hernandez-Sandoval [10] found that when 0.4 wt% Ni is added to the 354 alloy, Ni will react with Cu to form Al_3CuNi, which will occupy part of Cu and thus interfere with the formation of the Al_2Cu phase, which will affect the aging hardening process and reduce the tensile properties of the material; however, adding Zr alone or adding both Zr and Ni at the same time can improve the tensile properties of the alloy, especially at the aging temperature of 240 °C. The research of A.M.A. Mohamed [11] showed that the Zr-rich phase and the Ni-rich phase played an extremely important role in the fracture mechanism of the alloy. They added 0.2 wt% Zr and 0.2 wt% Ni to the 354 alloy and found that the UTS and YS of the alloy at 300 °C increased by about 70% and 39%, respectively. These results clearly prove that adding transition metal elements to the alloy can generate some thermally stable phases, thus improving the alloy's high-temperature performance; however, to date, the strengthening and toughening mechanism of transition metal elements is still not clear. What reaction has taken place between these transition metal elements and the main alloy elements of the base alloy, and what stable intermetallic phase has played a key role in the improvement of the high-temperature performance needs further research and revelation.

In our research, we began by comparing the base alloy and the alloy with the added transition metal elements. Then, we determined the strengthening effect of the modified alloy and discovered the intermetallic phases that played key roles in improving the high-temperature performance, as well as attempting to reveal its strengthening mechanism.

2. Materials and Methods

The experimental alloys were prepared in a graphite crucible resistance furnace by melting commercial master alloys of Al-20Si, Al-40Cu, Al-5Ti-B, Al-10Sr, Al-20Cr, Al-6Ti, Al-20V, Al-10Zr, Al-6Mo, and Al-10Mn in wt% and pure Al, Mg, and Zn metals to achieve the selected alloy chemistry, as listed in Table 1. The base alloy without the transition metal element is named BA, and the alloy with the transition metal-element is named MA.

Table 1. The chemistry of the base and modified alloy with addition of transition metal element (wt%).

Alloy	Si	Cu	Mg	Zn	Fe	Sr	Cr	Ti	V	Zr	Mo	Mn	Al
BA	9.1	0.94	0.38	0.61	0.15	0.005	-	0.15	-	-	-	-	Bal.
MA	8.8	0.90	0.41	0.59	0.16	0.005	0.37	0.42	0.29	0.31	0.29	0.31	Bal.

After casting, the test bar was heat treated. The test bars were divided into two groups: one group was heat treated with the solid solution treatment; the other group was heat treated with the aging treatment after the solution treatment. The solution temperature of the test bars with only the solution treatment was set to 500, 520, 540, and 560 °C. The heat treatment process for the other test bars was applying the solution treatment at 500 °C for 4 h and 520 °C for 5 h, followed by quenching in water at 60 °C, then applying aging treatment at 90 °C for 3 h and at 180 °C for 6 h. All test bars were processed and formed according to GB/T 6397-86 (Chinese Standard for Metal tensile

test specimen) Metallic materials—Test pieces for tensile testing, as shown in Figure 1. After processing, the tensile test was carried out on the test bars. The corresponding relationship between heat treatment and tensile test temperature is shown in Table 2. The high temperature tensile test was carried out on electronic universal testing machine (DDL100, Changchun Institute of Mechanical Science Co., Ltd, Changchun, China), with the test temperature of 25, 80, 160, 240, and 300 °C, and the tensile speed of 2 mm/min. Before the tensile test, the bars were heated to the test temperature in the heating chamber at a speed of 10 °C/min, and kept for 10 min. After stretching, the specimen was cut off 2 mm below the fracture surface by electrical discharge machining, polished and etched with Keller reagent (5 mL HNO3 + 3 mL HCL + 2 mL HF + 190 mL deionized water), and then carried out with Leica (DM2700M, Leica microsystems Co., Ltd, Wetzlar, Germany) optical microscope equipped with ISA4 metallographic image quantitative analysis system and Zeiss (SUPRA55, CarlZeiss AG, Oberkochen, Germany) scanning electron microscope equipped with Energy Disperse System.
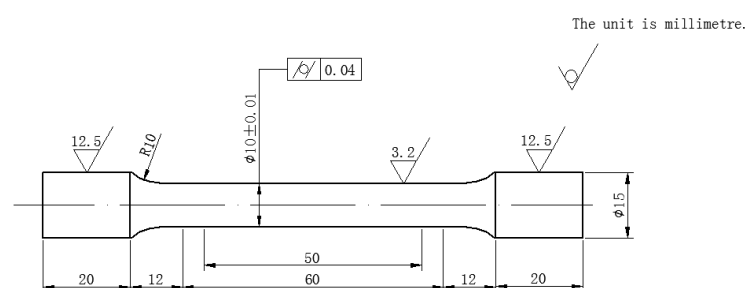

Figure 1. Shape and size of the high-temperature tensile specimen.

Table 2. The corresponding relationship between heat treatment and tensile test temperature.

Tensile Test Temperature	25 °C	80 °C	160 °C	240 °C	300 °C
Only solution treatment (500, 520, 540 and 560 °C)	✓				
Solution + quenching in water + aging treatment	✓	✓	✓	✓	✓

3. Results

3.1. Microstructural Analysis

The microstructure of the MA in the as-cast state is shown in Figure 2. The intermetallic phases calculated from EDS point analysis, intermetallic phases referenced by literature and morphology analysis are given in Table 3. Compared with BA, we found 13 new intermetallic phases in MA. They are $Al_{43.1}Si_{22.5}Cr$ (6#), $Al_{18.5}Si_{7.3}Cr_{2.6}V$ (7#), $Al_{7.9}Si_{8.5}Cr_{6.8}V_{4.1}Ti$ (8#), $Al_{10.7}SiTi_{3.6}$ (9#), $Al_{6.7}Si_{1.2}TiZr_{1.8}$ (10#), $Al_{21.4}Si_{3.4}Ti_{4.7}VZr_{1.8}$ (11#), $Al_{14.7}Si_{2.2}Mn_{4.5}Fe$ (12#), $Al_{38.2}Si_7Mn_{2.5}Mo_{4.6}Fe$ (13#), $Al_{67.8}Si_{8.3}Mn_{5.2}Fe_3Mo_{1.1}Cu$ (14#), $Al_{74.1}Si_{5.7}Mn_{3.6}Cr_{2.1}Fe$ (15#), $Al_{86.3}Si_{5.1}Mn_{2.1}Mo_{2.4}Cr_{1.4}Fe$ (16#), $Al_{8.4}Si_{24.1}Ti_{2.3}V_{3.3}Mo_{10.7}Cr$ (17#) and $Al_{13}Si_{50}Ti_{5.9}V_{8.4}Cr_{6.1}Mo_{13.8}$ (18#). The basic intermetallic phases consisted of α-Al dendrites (1#), Al–Si eutectic (2#), Al_2Cu with granular and blocky-shapes (3#,4#), and Q-$Al_5Cu_2Mg_8Si_6$ (5#). By searching references and comparing, $Al_{43.1}Si_{22.5}Cr$ (6#), $Al_{18.5}Si_{7.3}Cr_{2.6}V$ (7#), and $Al_{7.9}Si_{8.5}Cr_{6.8}V_{4.1}Ti$ (8#) belong to the CrVTi rich phase [8–12]; $Al_{10.7}SiTi_{3.6}$ (9#), $Al_{6.7}Si_{1.2}TiZr_{1.8}$ (10#), and $Al_{21.4}Si_{3.4}Ti_{4.7}VZr_{1.8}$ (11#) belong to TiVZr rich phase [11–13]; $Al_{14.7}Si_{2.2}Mn_{4.5}Fe$ (12#), $Al_{38.2}Si_7Mn_{2.5}Mo_{4.6}Fe$ (13#), $Al_{67.8}Si_{8.3}Mn_{5.2}Fe_3Mo_{1.1}Cu$ (14#), $Al_{74.1}Si_{5.7}Mn_{3.6}Cr_{2.1}Fe$ (15#), and $Al_{86.3}Si_{5.1}Mn_{2.1}Mo_{2.4}Cr_{1.4}Fe$ (16#) belong to the MoMnFe rich phase [9–14]; $Al_{8.4}Si_{24.1}Ti_{2.3}V_{3.3}Mo_{10.7}Cr$ (17#) and $Al_{13}Si_{50}Ti_{5.9}V_{8.4}Cr_{6.1}Mo_{13.8}$ (18#) belong to the TiVMo rich phase [15].
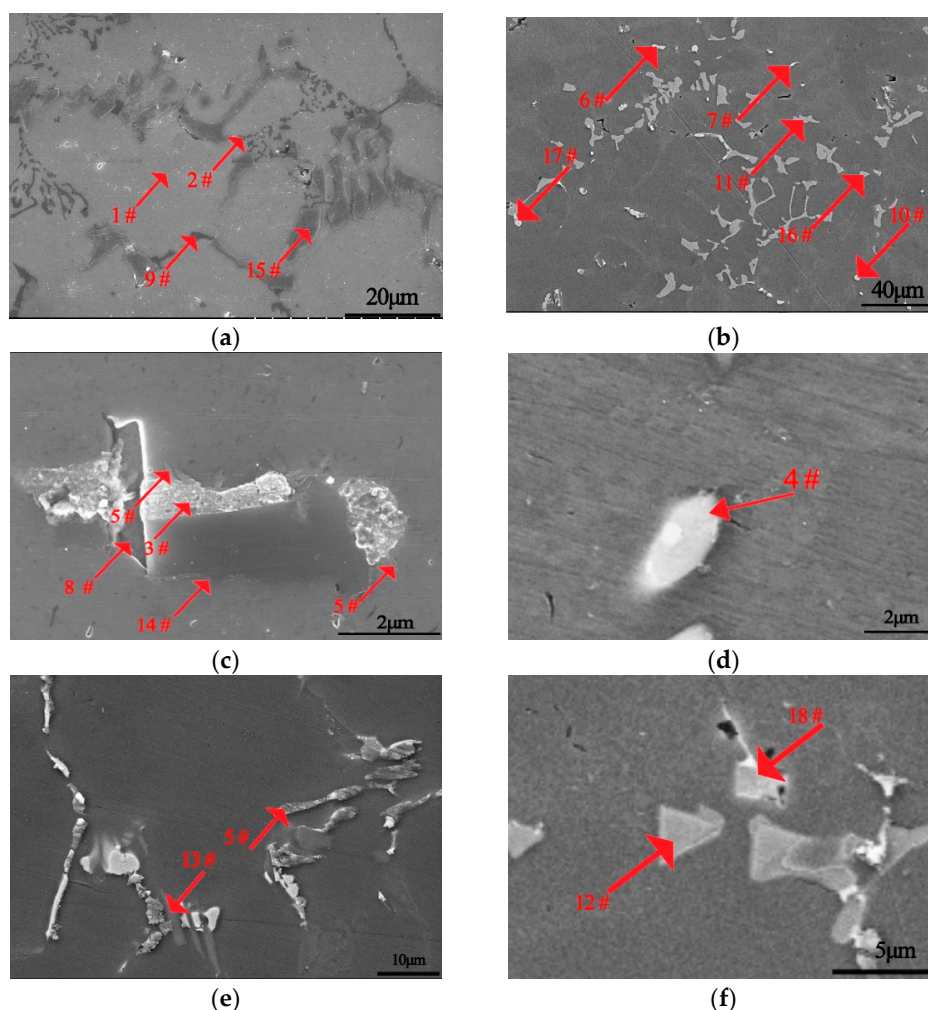
Figure 2. The as-cast microstructure of Al-9Si-1.2 Cu-0.4Mg-0.6Zn modified alloy by transition metal elements Cr, Ti, V, Zr, Mo, and Mn photographed under SEM, (**a**), (**b**), (**c**), (**d**), (**e**), (**f**): α-Al, eutectic Si and various intermetallic phases detailed in Table 3.

Table 3. Computed intermetallic phases of EDS detection, intermetallic phases of literature reference, and morphology analysis of Al-9Si-1.2Cu–0.4Mg-0.6Zn alloy added with transition metal element Cr-Zr-Ti-V-Mo-Mn.

No.	Calculation Phase from EDS Detection Components	Suggested Phase in the Literature	Response during T6 Temper	Phase Morphology
1#	α-Al	α-Al	No change	Dendritic
2#	Eutectic Si	Eutectic Si	Partially dissolved	Fibrous like
3#	$Al_{2.7}Cu_{0.4}$	Eutectic Al_2Cu	Dissolved	Granular
4#	$Al_{3.2}Cu_{0.6}$	Blocky Al_2Cu	Dissolved	Blocky
5#	$Al_9Si_{1.1}Cu_{1.1}Mg$	$Q-Al_5Cu_2Mg_8Si_6$	Partially dissolved	Needle-like
6#	$Al_{43.1}Si_{22.5}Cr$	$(AlSi)_3Cr$	Partially dissolved	Needle-like
7#	$Al_{18.5}Si_{7.3}Cr_{2.6}V$	$(AlSi)_3(CrV)$	Partially dissolved	Needle-like
8#	$Al_{7.9}Si_{8.5}Cr_{6.8}V_{4.1}Ti$	$(AlSi)_3(CrVTi)$	No change	Plate
9#	$Al_{10.7}SiTi_{3.6}$	$(AlSi)_3Ti$	No change	Blocky
10#	$Al_{6.7}Si_{1.2}TiZr_{1.8}$	$(AlSi)_3(TiZr)$	Partially dissolved	Blocky
11#	$Al_{21.4}Si_{3.4}Ti_{4.7}VZr_{1.8}$	$(AlSi)_3(TiVZr)$	No change	Blocky
12#	$Al_{14.7}Si_{2.2}Mn_{4.5}Fe$	$α-Al_{17}Fe_{3.2}Mn_{0.8}Si_2$	Partially dissolved	Blocky
13#	$Al_{38.2}Si_7Mn_{2.5}Mo_{4.6}Fe$	$Al_{0.78}Fe_{4.8}Mn_{0.27}Mo_{4.15}Si_2$	No change	Strip
14#	$Al_{67.8}Si_{8.3}Mn_{5.2}Fe_3Mo_{1.1}Cu$	$Al_{65}Cu_{20}Fe_6Mn$	Completely dissolved	Plate
15#	$Al_{74.1}Si_{5.7}Mn_{3.6}Cr_{2.1}Fe$	$Al_{74}Si_6Mn_4Cr_2Fe$	No change	Chinese script
16#	$A_{86.31}Si_{5.1}Mn_{2.1}Mo_{2.4}Cr_{1.4}Fe$	$Al_{85}Si_5Mn_2Mo_2CrFe$	No change	Granular
17#	$Al_{8.4}Si_{24.1}Ti_{2.3}V_{3.3}Mo_{10.7}Cr$	$(AlSi)_2(CrVTi)Mo$	No change	Blocky
18#	$Al_{13}Si_{50}Ti_{5.9}V_{8.4}Cr_{6.1}Mo_{13.8}$	$Al_{13}(MoCrVTi)_4Si_4$	No change	Blocky

Figure 3 shows the XRD analysis of the BA and the MA added with the transition metal elements. The existence of α-Al and eutectic silicon was confirmed by comparing the diffraction peaks; the corresponding peaks are marked with squares and triangles, respectively. The diffraction peaks corresponding to the rich TiVZr phase, rich CrVTi phase, and rich MoMnFe phase were found through the amplification of the diffraction peaks, which were named $(AlSi)_x(TiVZr)$, $(AlSi)_x(CrVTi)$, and $(AlSiMnFe)_x(MoCr)$ phases, and the corresponding peaks were marked with a diamond, star, and pentagram, respectively. This result is consistent with the results determined by EDS and compared with the results determined by literature. However, due to the small amount of transition alloy elements, the diffraction peaks in XRD patterns are low, and because of the existence of some impurity peaks, it is difficult to distinguish the specific intermetallic phases.
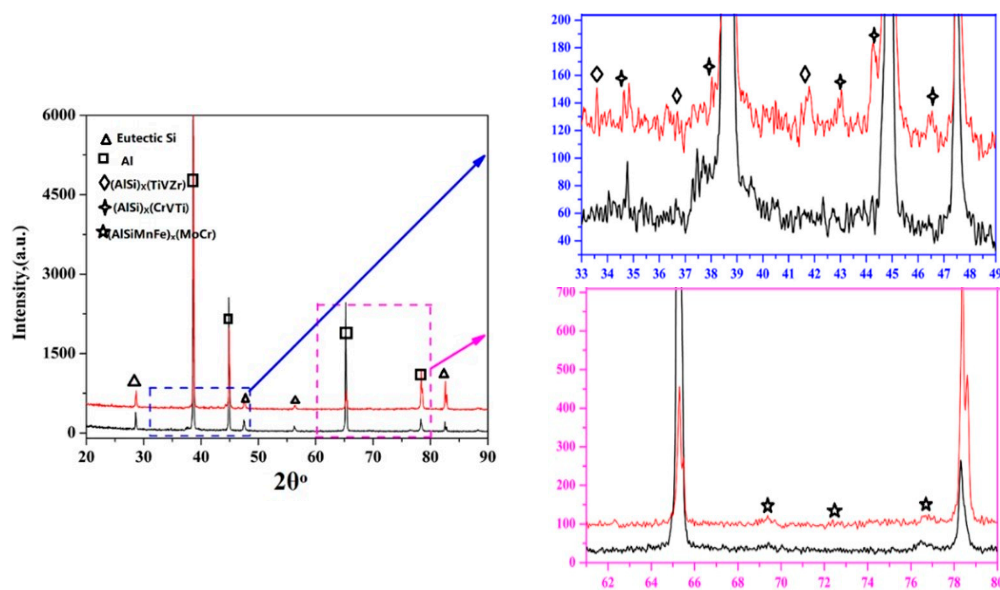

Figure 3. XRD patterns of the base alloy without the transition metal element (BA) and the alloy with the transition metal element (MA).

In order to characterize the failure mechanisms, electrical discharge machining was used to cut the bar parallel to the tensile axis to expose the center of the cylindrical bar, and ground and polished the cut surface. Through observation, four kinds of intermetallic phases were found in the fracture. These four kinds of intermetallic phases are $Al_{74}Si_6Mn_4Cr_2Fe$ (15#), $Al_{85}Si_5Mn_2Mo_2CrFe$ (16#), $Al_{13}(MoCrVTi)_4Si_4$ (18#), and $(AlSi)_2$-$(CrVTi)Mo$ (17#), corresponding to Figure 4a–d. According to the fracture characteristics, the matrix near the $Al_{74}Si_6Mn_4Cr_2Fe$ (15#) phase (Figure 4a) and $Al_{85}Si_5Mn_2Mo_2CrFe$ (16#) phase (Figure 4b) breaks with the intermetallic phase, and the fracture of the $Al_{13}(MoCrVTi)_4Si_4$ (18#) phases occurs with the macro crack across the test bar (Figure 4c); however, the fracture of the $(AlSi)_2(CrVTi)Mo$ (17#) phase is different (Figure 4d). After the fracture of the test bar, the morphology of $(AlSi)_2(CrVTi)Mo$ (17#) phase is complete, and the fracture path is along the boundary of $(AlSi)_2(CrVTi)Mo$ (17#) phase.

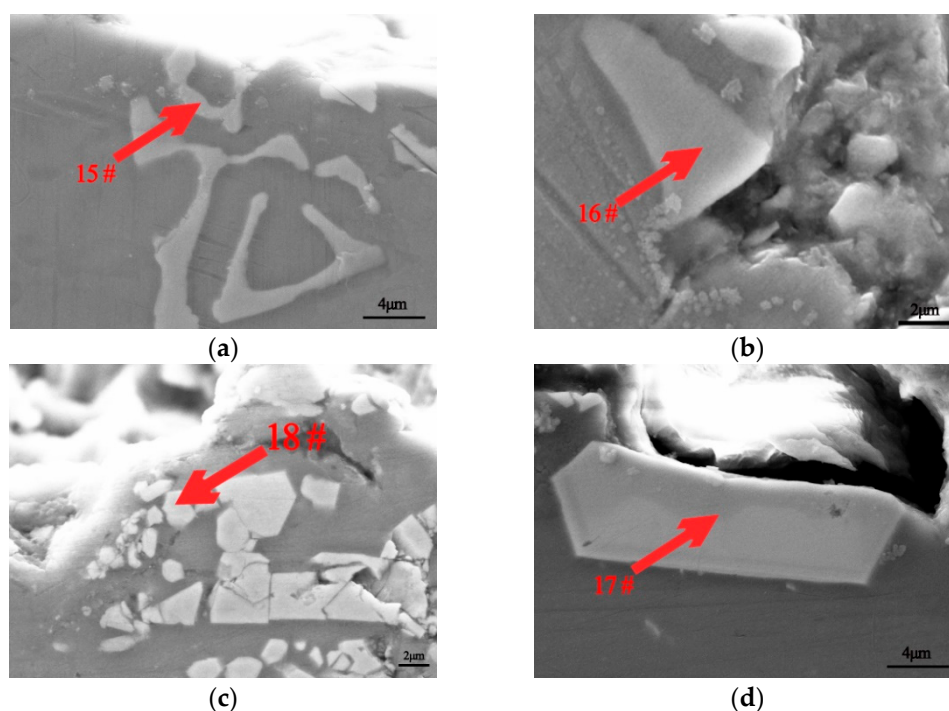**Figure 4.** Intermetallic phases of MA found at facture by SEM: (**a**) $Al_{74}Si_6Mn_4Cr_2Fe$ phase (15#); (**b**) $Al_{85}Si_5Mn_2Mo_2CrFe$ phase (16#); (**c**) $Al_{13}(MoCrVTi)_4Si_4$ phase (18#); (**d**) $(AlSi)_2(CrVTi)Mo$ phase (17#).

3.2. Alloy Tensile Properties

The tensile properties of the BA and MA, heat-treated at different solution temperatures of respectively 500, 520, 540, and 560 °C for 6 h, were tested at room temperature and are shown in Figure 5. The heat treatment process of the test bar used for testing here is the solution-only treatment. The results show that the UTS, YS, and percent elongation (%EL) all increase at first and then decrease with the increase in solution temperatures and reach the peak at 520 °C. It is worth noting that when the solution treatment temperature is higher than 520 °C, although the tensile properties of the two alloys tend to decline, the tensile properties of the BA decrease much faster than that of the MA at room temperature.
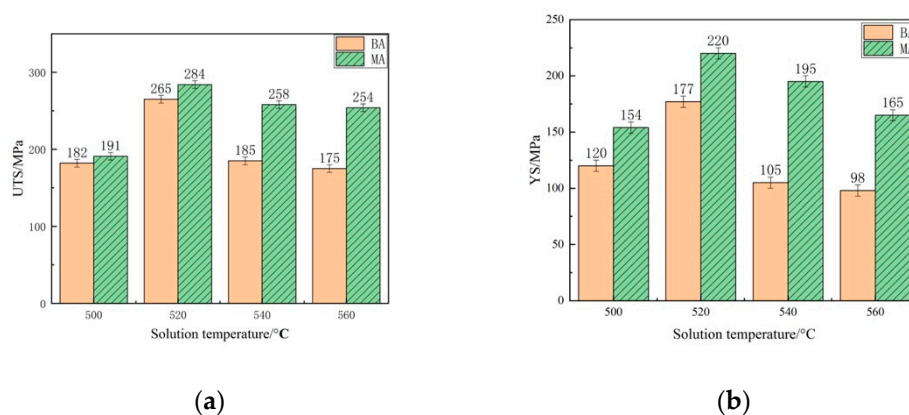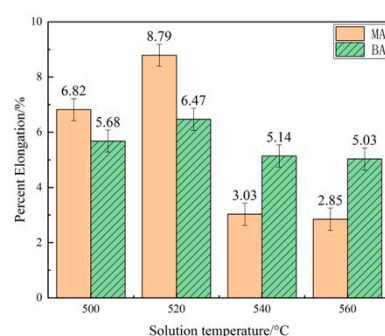

Figure 5. *Cont*.

(**c**)

Figure 5. The influence of solution temperature on the mechanical properties of BA and MA at room temperature: (**a**) ultimate tensile strength (UTS); (**b**) yield strength (YS); (**c**) elongation percent (%EL).

Tensile tests were carried out at different temperatures (25, 80, 160, 240, and 300 °C) after the T6 heat treatment (solution and ageing heat treatment) of the two alloys, and the obtained data are shown in Figure 6. Obviously, with the increase in test temperature, the UTS and YS of the alloy show a decreasing trend, while the %EL of the alloy increases with the increase in temperature. It is worth mentioning that the strength values (UTS, YS) of the MA are better than those of the BA in all test temperature ranges (25–300 °C). In addition, the reduction response of the BA strength value significantly changed at 160 °C. Taking 160 °C as the critical temperature, the calculated change value of performance reduction response is shown in Table 4. Obviously, when the temperature is lower than 160 °C, the performance reduction response of the two alloys is almost the same. When the temperature is higher than 160 °C, the advantage of MA alloy is obvious.
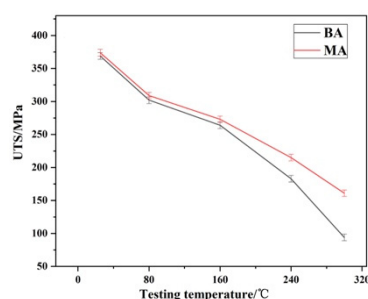
(**a**)
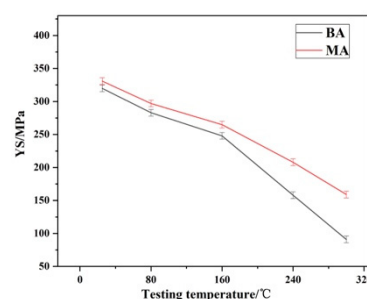
(**b**)
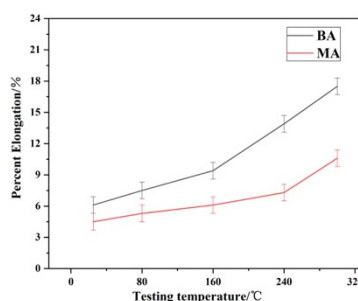
(**c**)

Figure 6. Tensile properties of alloys BA and MA at different test temperatures: (**a**)UTS; (**b**)YS; (**c**) %EL.

Table 4. The performance reduction response of the two alloys for every 10 °C increase in temperature range.

	UTS/MPa (<160 °C)	UTS/MPa (>160 °C)	YS/MPa (<160 °C)	YS/MPa (>160 °C)	%EL (<160 °C)	%EL (>160 °C)
BA	6.6	12.1	4.5	11.2	−0.21%	−0.55%
MA	6.3	8.1	4.2	7.6	−0.11%	−0.32%

Compared to the BA, the UTS and YS of the MA are only increased by 1.36% and 3.44% at room temperature, 3.41% and 6.85% at 160 °C, 17.49%, and 31.65% at 240 °C respectively; when the temperature rises to 300 °C, the UTS and YS are increased by 71.28% and 74.73%, respectively.

3.3. Thermal Stability Analysis of Alloy Elements

SEM/EDS facial scanning was carried out to investigate the thermal stability of the intermetallic phases in the MA and to observe and judge whether the elements could remain in the aggregation state or whether the phenomenon of dissolution and homogenization occurred. The scanning object is the sample containing eight alloying elements Cu, Mg, V, Zr, Ti, Cr, Mn, and Mo, which were heat-treated at the solution temperature of 500, 520, 540, and 560 °C, respectively. The scanning results are shown in Figure 7. The Cu and Mg atomic groups have been partially dissolved at 500 °C for 6 h, whereas the Cu and Mg atoms are completely dissolved and homogenized when the temperature rises to 520 °C. The atomic groups of V, Zr, and Ti can keep aggregation at 520 °C, but when the temperature rises to 540 °C, the atomic groups of V, Zr, and Ti are dissolved and homogenized, and their thermal stability lost. Compared with the above-mentioned five elements, Cr, Mn, and Mo have better thermal stability, and the atomic groups of the three elements still do not dissolve and homogenize after being kept at 560 °C for 6 h, and can remain aggregated.
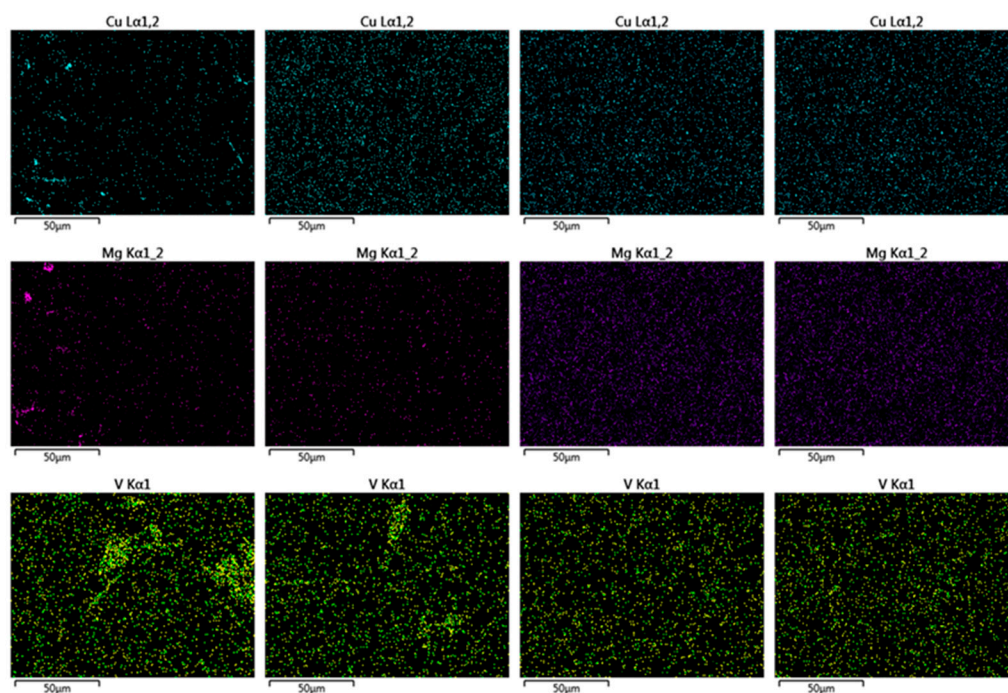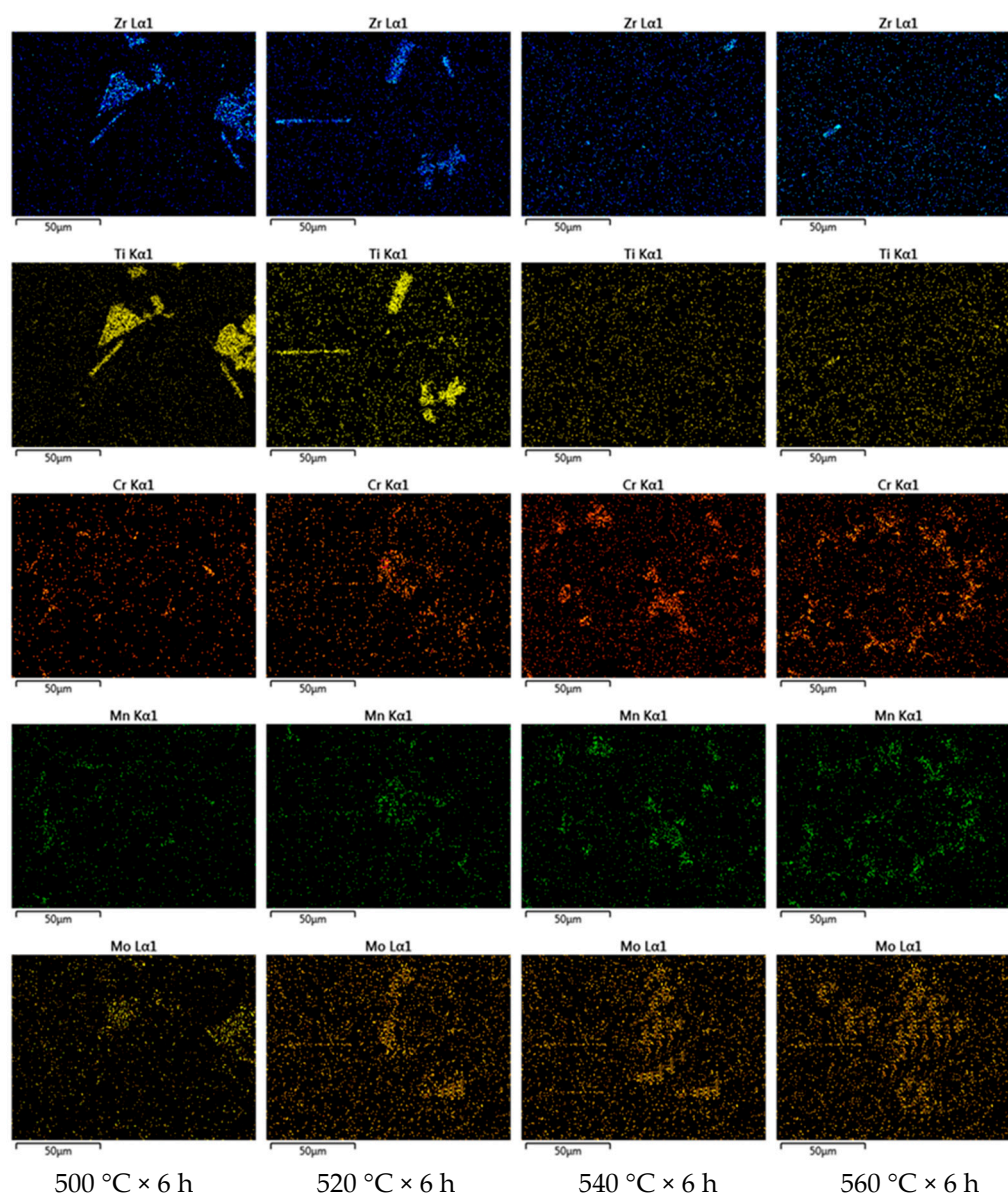

Figure 7. *Cont.*

Figure 7. Analysis of atomic thermal stability of V, Zr, Ti, Cr, Mn, and Mo.

4. Discussion

In Section 3.3, it was observed that Cu and Mg atomic groups have been partially dissolved at 500 °C, whereas Cu and Mg atomic groups are completely dissolved and homogenized when the temperature is raised to 520 °C for 6 h. This result clearly shows that the thermal stability of the Cu-rich phase and the Mg-rich phase is poor, and it can also explain why the traditional Al–Si–Cu–Mg alloy has excellent properties at room temperature—its mechanical properties will greatly decrease when the temperature rises. In other words, it is precisely because the Cu and Mg atoms have been diffused and homogenized, and this phenomenon will inevitably lead to the dissolution of rich Cu phase and rich Mg phase, which cannot have a beneficial effect on the high-temperature properties of the alloy. These phases are mostly present in the traditional intermetallic phase, such as Al_2Cu, Mg_2Si, and Q-$Al_5Cu_2Mg_8Si_6$, which plays a strengthening role at room temperature. This shows that Cu and Mg atoms have adverse effects on the high-temperature stability of the intermetallic phase. In comparison, because V, Zr, and Ti atomic groups can keep aggregation at a higher temperature, the thermal stability of intermetallic phases rich V, Zr, and Ti must also be improved; Cr, Mn, and Mo atoms have higher thermal stability,

without dissolution, even at 560 °C. It can be inferred that the thermal stability of the new intermetallic phases should be higher than that of the traditional intermetallic phases due to the presence of V, Zr, Ti, Cr, Mn, and Mo atoms, especially Cr, Mn, and Mo atoms.

During the microstructure analysis, it was found that V, Zr, and Ti atoms mainly exist in the rich TiVZr phase, whereas Cr, Mn, and Mo atoms are mainly distributed in the rich CrVTi phase, rich TiVMo phase, and rich MoMnFe phase. It was found that the rich TiVZr phase will lose its thermal stability when working at 540 °C or above, whereas the rich CrVTi phase, rich TiVMo phase, and rich MoMnFe phase cannot dissolve and homogenize under the working conditions of ≤580 °C and keep the aggregation state of atoms with good thermal stability. Those phases all have good thermal stability, which can greatly promote the high temperature properties of the alloy.

In Section 3.2, it was observed that the peak tensile properties of both BA and MA appeared at the solution temperature of 520 °C. When the solution temperature is higher than 520 °C, the tensile properties of both alloys tend to decline, but UTS and YS of the MA increased by 7.17% and 24.29%, respectively, and the %EL decreased by 26.39%. When the solution temperature raised to 540 °C, the UTS and YS of the modified alloy MA increased by 39.46% and 85.71%, respectively, compared with the BA, and the %EL increased by 69.64% compared with the BA. Based on the SEM/EDS scanning results of Cu and Mg atoms in Section 3.3, the reason for this phenomenon is that the Cu and Mg atomic groups in Al–Si–Cu–Mg alloy have been dissolved and homogenized at 520 °C, and the main strengthening phases, Al_2Cu phase (3#,4#), and Q-$Al_5Cu_2Mg_8Si_6$ phase (5#) have been dissolved, so the tensile properties of the alloy will be improved. The melting point of the Al_2Cu phase is 523 °C, and the melting point of the Q-$Al_5Cu_2Mg_8Si_6$ phase is 533 °C; therefore, when the alloy is kept at a temperature higher than this temperature for a long time, the traditional microstructure which can improve the tensile properties at room temperature has almost completely dissolved, which can not hinder the migration of dislocation [16], and the tensile properties of BA alloy decrease sharply. The intermetallic phases, such as the rich CrVTi phase, rich TiVMo phase, rich MnMoFe phase, and rich TiVZr phase contained in MA, can exist stably and do not dissolve at high temperatures; these intermetallic phases are pinned at the grain boundary, so the diffusion deformation of the grain boundary can be hindered to a certain extent, thus preventing the generation of microcracks. There is also a large transition in the reduction response of tensile properties of BA and a small transition of MA when the solution temperature is above 520 °C. Similarly, when stretching at a high temperature, the bonding force between the matrix material and the second phase will become weak with the increase in solution temperature. For some traditional intermetallic phases, the adjacent relationship between atoms will be lost at 160 °C, and the grain boundary will undergo diffusion deformation, which will greatly reduce the alloy's mechanical properties; however, even though some traditional second phases in MA with transition metal elements are in an unstable state, due to the existence of high-temperature stable phases, defects such as dislocation can still be hindered, so that the strength index of the alloy can still maintain a high level.

In terms of the fracture mechanism, in plastic deformation, the strength of the intermetallic phase is much greater than that of the matrix, so the intermetallic phase can play a role in preventing the slip. As a result of the slip, stress concentration occurs at the boundary between the intermetallic phase and the slip plane. With the increase in strain, the more dislocations in the plug group, the more stress concentration. When the concentrated stress is equal to the strength of the intermetallic phase, it will lead to the fracture of the intermetallic phase. Compared with the direct fracture of the matrix, the fracture process of the intermetallic phase needs more energy, which increases the difficulty of material fracture; therefore, the existence of the $Al_{13}(MoCrVTi)_4Si_4$ (18#) phase can increase the fracture limit of the material; however, at the same time, many secondary cracks were observed in the $Al_{13}(MoCrVTi)_4Si_4$ (18#) phase, which indicates that the $Al_{13}(MoCrVTi)_4Si_4$ (18#) phase is still brittle. This means that although the $Al_{13}(MoCrVTi)_4Si_4$ (18#) phase can increase the high-temperature tensile properties of the alloy, it will also reduce the toughness of the alloy.

The $Al_{74}Si_6Mn_4Cr_2Fe$ (15#) and $Al_{85}Si_5Mn_2Mo_2CrFe$ (16#) phases are also brittle phases. Although the $Al_{74}Si_6Mn_4Cr_2Fe$ (15#) and $Al_{85}Si_5Mn_2Mo_2CrFe$ (16#) phases also fracture, there is no secondary crack on the phases, which means that the brittleness of the $Al_{74}Si_6Mn_4Cr_2Fe$ (15#) and $Al_{85}Si_5Mn_2Mo_2CrFe$ (16#) phases is less than the $Al_{13}(MoCrVTi)_4Si_4$ (18#) phase. It also shows that the toughness of the $Al_{74}Si_6Mn_4Cr_2Fe$ (15#) and $Al_{85}Si_5Mn_2Mo_2CrFe$ (16#) phases decreases by less than that of the alloy. It is worth noting that the morphology of the $(AlSi)_2(CrVTi)Mo$ (17#) phase is complete, and the fracture path is along the boundary of $(AlSi)_2(CrVTi)Mo$ (17#) phase. When the fracture behavior reaches the $(AlSi)_2(CrVTi)Mo$ (17#) phase, it can prevent the extension of dislocation. Because of its good plasticity, the intermetallic phase does not break, so the crack can only extend along the morphological boundary of the $(AlSi)_2(CrVTi)Mo$ (17#) phase, which increases the energy needed for fracture, and has a positive effect on its strength but no negative effect on the toughness index of materials. It thus is proven that the $(AlSi)_2(CrVTi)Mo$ (17#) phase has a positive effect on the strength and plasticity of the material.

5. Conclusions

The MA was prepared by adding the transition metal elements Cr, Ti, V, Zr, Mo, and Mn into BA. Based on the data obtained by a tensile test after treatment at different solution temperatures and a high-temperature tensile test at different test temperatures, the following conclusions can be drawn:

Although transition metal elements are added to MA, the tensile properties of both alloys reach a peak at 520 °C. When the solution temperature is higher than 520 °C, the decrease in tensile properties of MA is much slighter than that of BA.

At all test temperatures (25–300 °C), the strength values of MA with transition metal elements are better than that of BA, and this advantage will be more obvious when the test temperature is higher than 160 °C. Compared with BA, the UTS and YS of the MA increased by only 1.36% and 3.44% at room temperature, 3.41% and 6.85% at 160 °C, 17.49% and 31.65% at 240 °C, and 71.28% and 74.73% at 300 °C, respectively.

The addition of transition metal elements Cr, Ti, V, Zr, Mo, and Mn changed the microstructure of the Al–Si–Cu–Mg alloy. Based on the inherent basic intermetallic phases, there are 13 kinds of intermetallic phases, such as the rich TiVZr phase: $(AlSi)_3(TiVZr)$, $(AlSi)_3(TiZr)$, and $(AlSi)_3Ti$; the rich CrVTi phase: $(AlSi)_3(CrV)$, $(AlSi)_3Cr$, and $(AlSi)_3(CrVTi)$; the rich MoMnFe phase: α-$Al_{17}Fe_{3.2}Mn_{0.8}Si_2$, $Al_{0.78}Fe_{4.8}Mn_{0.27}Mo_{4.15}Si_2$, $Al_{65}Cu_{20}Fe_6Mn$, $Al_{74}Si_6Mn_4Cr_2Fe$, and $Al_{85}Si_5Mn_2Mo_2CrFe$; the rich CrVTi phase: $(AlSi)_2(CrVTi)Mo$ and $Al_{13}(MoCrVTi)_4Si_4$. Among them, the intermetallic phases that can exist stably at high temperatures are $(AlSi)_3(TiVZr)$, $(AlSi)_3Ti$, $(AlSi)_3(CrVTi)$, $Al_{74}Si_6Mn_4Cr_2Fe$, $Al_{85}Si_5Mn_2Mo_2CrFe$, $Al_{0.78}Fe_{4.8}Mn_{0.27}Mo_{4.15}Si_2$, $(AlSi)_2(CrVTi)Mo$, and $Al_{13}(MoCrVTi)_4Si_4$.

Cu and Mg atomic groups were partially dissolved at 500 °C, and can be completely dissolved and homogenized when the temperature reaches 520 °C; Zr, V, and Ti atomic groups can still remain aggregated at 520 °C, and begin to dissolve and homogenize when the temperature is higher than 520 °C; however, Cr, Mo, and Mn atomic groups can remain aggregated at 560 °C without dissolution.

The intermetallic phases containing transition metal elements can exist stably at high temperature, and the thermal stability of the rich MoMnFe, rich TiVMo, and rich CrVTi phases is better than that of the rich TiVZr phase. When the alloy works at a high temperature, the traditional phases lose its strengthening effect, but due to these high-temperature stable phases, it can still hinder the defects such as dislocation, so that the strength index of the alloy can still maintain a high level.

The $Al_{74}Si_6Mn_4Cr_2Fe$, $Al_{85}Si_5Mn_2Mo_2CrFe$, $Al_{13}(MoCrVTi)_4Si_4$, and $(AlSi)_2(CrVTi)Mo$ phases have a positive effect on the tensile strength of the alloy at high temperature; however, compared with the other three phases, the $(AlSi)_2(CrVTi)Mo$ phase can improve the tensile strength of the alloy and has no negative effect on the plasticity of the alloy.

References

1. Patrik, H.; Stefan, O. Thermo-mechanical fatigue influence of copper and silicon on hypo-eutectic Al–Si–Cu and Al–Si–Mg cast alloys used in cylinder heads. *Int J Fatigue* **2016**, *88*, 142–155. [CrossRef]
2. Jovid, R.; Liu, K. Enhanced mechanical properties of high-temperature-resistant Al–Cu cast alloy by microalloying with Mg. *J. Alloy. Compd.* **2020**, *827*, 154–162. [CrossRef]
3. Saïd, B.; Zakaria, B. Effects of heat treatment and addition of small amounts of Cu and Mg on the microstructure and mechanical properties of Al-Si-Cu and Al-Si-Mg cast alloys. *J. Alloy. Compd.* **2019**, *784*, 1026–1035. [CrossRef]
4. Zheng, Y.; Xiao, W.L. Effects of Cu content and Cu/Mg ratio on the microstructure and mechanical properties of Al–Si–Cu–Mg alloys. *J. Alloy. Compd.* **2015**, *649*, 291–296. [CrossRef]
5. Mørtsell, E.A.; Qian, F. Precipitation in an A356 foundry alloy with Cu additions - A transmission electron microscopy study. *J. Alloy. Compd.* **2019**, *785*, 1106–1114. [CrossRef]
6. Li, R.X.; Li, R.D.; Lu, W. Role of Cu and Mg in the aging process of al-Si-Cu-mg alloy casting. In Proceedings of the first International Casting Grand View Park and the seventh Foundry Industry and Trade Conference, Guilin, China, 16–20 September 2007; pp. 377–383.
7. Shaha, S.K.; Czerwinski, F. Effect of Cr, Ti, V, and Zr Micro-additions on Microstructure and Mechanical Properties of the Al-Si-Cu-Mg Cast Alloy. *Metall. Mater. Trans.* **2016**, *47*, 2396–2409. [CrossRef]
8. Shaha, S.K.; Czerwinski, F. Ageing characteristics and high-temperature tensile properties of Al–Si–Cu–Mg alloys with micro-additions of Cr, Ti, V and Zr. *Mater. Sci. Eng. A* **2016**, *652*, 353–364. [CrossRef]
9. Shaha, S.K.; Czerwinski, F. Ageing characteristics and high-temperature tensile properties of Al–Si–Cu–Mg alloys with micro-additions of Mo and Mn. *Mater. Sci. Eng. A* **2017**, *684*, 726–736. [CrossRef]
10. Hernandez-Sandoval, J.; Garza-Elizondo, G.H. The ambient and high temperature deformation behavior of Al–Si–Cu–Mg alloy with minor Ti, Zr, Ni additions. *Mater. Des.* **2014**, *58*, 89–101. [CrossRef]
11. Mohamed, A.M.A.; Samuel, F.H. Microstructure, tensile properties and fracture behavior of high temperature Al–Si–Mg–Cu cast alloys. *Mater. Sci. Eng. A* **2013**, *577*, 64–72. [CrossRef]
12. An, Z.H.; Yang, W.H. On the strengthening effect of Al-Cr-Si dispersoid in an Al-Si-Mg-Cu casting alloy with Cr addition. *Mater. Charact.* **2020**, *166*, 110–122. [CrossRef]
13. Liu, G.Y.; Blake, P. Effect of Zr on the high cycle fatigue and mechanical properties of Al–Si–Cu–Mg alloys at elevated temperatures. *J. Alloy. Compd.* **2019**, *809*, 151–264. [CrossRef]
14. Giordano, C.; Giulio, T. Grain refinement of gravity die cast secondary AlSi7Cu3Mg alloys for automotive cylinder heads. *Trans. Nonferrous Met. Soc. China* **2016**, *26*, 1211–1221. [CrossRef]
15. Shaha, S.K.; Czerwinski, F. Effect of Mn and heat treatment on improvements in static strength and low-cycle fatigue life of an Al–Si–Cu–Mg alloy. *Mater. Sci. Eng. A* **2016**, *657*, 441–452. [CrossRef]
16. Zuo, L.J.; Ye, B. Effect of Q-$Al_5Cu_2Mg_8Si_6$ phase on mechanical properties of Al-Si-Cu-Mg alloy at elevated temperature. *Mater. Sci. Eng. A* **2017**, *693*, 26–32. [CrossRef]